Comparison of Two Restoration Techniques in the Context of 3D Medical Imaging

Conference Paper · October 2001

DOI: 10.1007/3-540-45468-3_123 · Source: DBLP

4 authors:

Miguel Angel Rodriguez-Florido
Instituto Tecnológico de Canarias
24 PUBLICATIONS **213** CITATIONS
SEE PROFILE

Karl Krissian
Ecole normale supérieure de Cachan
71 PUBLICATIONS **2,200** CITATIONS
SEE PROFILE

Juan Ruiz-Alzola
Universidad de Las Palmas de Gran Canaria
94 PUBLICATIONS **1,229** CITATIONS
SEE PROFILE

Carl-Fredrik Westin
Harvard University
454 PUBLICATIONS **18,173** CITATIONS
SEE PROFILE

Comparison of two restoration techniques in the context of 3D medical imaging.

M.A. Rodriguez-Florido[1], K. Krissian[2], J.Ruiz-Alzola[1], and C-F. Westin[3]

[1] Departamento de Señales y Comunicaciones
[2] Departamento de Informatica y Sistemas †
Universidad de Las Palmas de Gran Canaria
Campus de Tafira, 35017 Las Palmas, Spain
[3] SPL-BWH-Harward Medical School
{marf,jruiz}@dsc.ulpgc.es; krissian@dis.ulpgc.es; westin@bwh.harvard.edu

Abstract. In this paper, we compare two restoration techniques applied to 3D angiographies and to femoral CT scans. The first technique uses a Partial Derivative Equation and the second one is based on an extension of adaptive Wiener filters. We first present each method. Then, we discuss and compare the estimation of the local orientations in 3D images obtained either by the smoothed gradient and the principal curvature directions or by the eigenvectors of the structure tensor. A good estimation of the orientations is essential because it leads the restoration process. Finally, we compare the restored images on both synthetic and real images for the two studied applications.

1 Introduction

Image enhancement is especially important in medical imaging, because this process allows assisting physicians for a better visual interpretation: view weak structures (i.e. thin vessels), difference false joint regions (i.e. space between femoral head and hip) and other numerous clinical applications. Moreover, enhancement is a preprocessing step for subsequent automated medical analysis, like segmentation of different tissues or registration of images from different modalities. In this sense, this paper presents a qualitative comparison between anisotropic diffusion [11, 13, 8] and anisotropic adaptive frequency filtering [7, 14], to show physicians and technicians their relative merits, and propose in futures work improvements or a feedback process between both. We have also compared the local structure estimation that every technique uses, analyzing which one is the best in different cases. The paper is structured as follows: first, we describe different methods to extract local structure; second, we present a brief description of both methods, and finally we present our results when comparing both techniques.

2 Presentation of the two methods

In this section, we present two 3D anisotropic filtering techniques. The first one is based on anisotropic diffusion and uses the gradient and the principal

† This work was partially founded by the European project on viscosity equations and their solutions.

curvature directions. The second one is designed in the Fourier domain and uses the eigenvectors of the structure tensor to drive the filtering.

2.1 Flux-Based Anisotropic Diffusion

In [9, 8], the author proposes a multi-directional flux-based diffusion scheme. The general expression of the diffusion equation is:

$$\begin{cases} u(x,0) = u_0 \\ \frac{\partial u}{\partial t} \quad = div(\mathbf{F}) + \beta(u_0 - u). \end{cases} \tag{1}$$

where $\mathbf{F}$ is the diffusion flux that drives the diffusion and β is a data attachment term which allows a convergence of the diffusion scheme to an image that remains close to the initial data. The expression of the differential equation as the divergence of a vector field ensures the conservation of the image intensity. Particular cases of this equation with $\beta = 0$ are:

- the heat diffusion equation $\mathbf{F} = \nabla u$ which is equivalent to a Gaussian convolution. In spite of the different invariance properties of this equation (translation, isometry, scaling) and its ability to reduce noise, the heat equation does not preserve the contours of the image and smoothes the information in an isotropic way regardless of the presence of contours.
- the Perona and Malik equation [11] with $\mathbf{F} = g(\parallel \nabla u \parallel)\nabla u$ where g is a diffusion function. This function has the effect of reducing the diffusion for 'high' gradients. To achieve this goal, a *threshold* δ on the norm of the gradient is introduced. g is chosen in such a way that it diffuses a little when $\parallel \nabla u \parallel$ is higher than δ ; and it tends to a positive constant when $\parallel \nabla u \parallel$ is close to zero, acting like the heat diffusion. However, the flux is always oriented in the gradient direction.
- the matrix diffusion proposed in [13], which uses a diffusion matrix noted D with a flux $\mathbf{F} = D\nabla u$. The matrix D can be expressed in a diagonal form, with eigenvectors $(\mathbf{v}_0, \mathbf{v}_1, \mathbf{v}_2)$ and eigenvalues $\lambda_0, \lambda_1, \lambda_2$. Then the flux can be expressed as $\mathbf{F} = D\nabla u = \sum_{i=0}^{2} \lambda_i u_{\mathbf{v}_i} \mathbf{v}_i$ where $u_{\mathbf{v}_i} = \nabla u.\mathbf{v}_i$ is the first order derivative of the intensity in the direction of $\mathbf{v}_i$.

Let $(\mathbf{e}_0, \mathbf{e}_1, \mathbf{e}_2)$ denote any orthogonal unit basis of $\mathbb{R}^3$ that generally depends on the local structures of the image, the diffusion flux proposed in [9, 8] for this basis is written as:

$$\mathbf{F} = \sum_{i=0}^{2} \phi_i(u_{\mathbf{e}_i})\mathbf{e}_i. \tag{2}$$

It is equivalent to a tensor diffusion where the eigenvectors of the diffusion matrix are $(\mathbf{e}_i)_{i\in\{0,1,2\}}$ and the eigenvectors are functions of the first order derivative of the intensity in the direction of the associated eigenvector: $\lambda_i = \lambda_i(u_{\mathbf{e}_i})$ leading to diffusion functions $\phi_i(u_{\mathbf{e}_i}) = \lambda_i(u_{\mathbf{e}_i})u_{\mathbf{e}_i}$. This choice allows to separate the diffusion in different directions so that the diffusion in a given direction does not depend on the intensity variations in the other directions. Some interpretation of this diffusion scheme is given in [9, 8] where its good behavior is shown in the case of enhancement of 3D angiographies.

For the local orientations, we use the gradient and principal curvature directions computed on the smoothed image u^*, where the smoothing is obtained by convolution with a Gaussian of standard deviation σ (as in [10]). This basis corresponds respectively to unit vectors in the directions of the gradient ($\mathbf{e}_0 = \frac{\nabla u^*}{\|\nabla u^*\|}$), and of the maximal and minimal curvature of the smoothed image. The principal curvature directions can be computed as two of the eigenvalues (resp. eigenvectors) of the matrix PHP where H is the Hessian matrix of the image and P is the projection matrix orthogonal to the gradient direction, that is $H' = PH_\sigma P$ with $P = I - \mathbf{e}_0\mathbf{e}_0{}^t$, where H_σ is the Hessian matrix of the smoothed image previously computed, I is the identity matrix in 3D. One of the eigenvectors of this matrix is the gradient of the smoothed image with a zero associated eigenvalue, and the two others are the directions of principal curvature.

The diffusion functions Φ_i of equ. (2) are chosen as $\Phi_0(x) = x\, e^{-(\frac{x}{\delta})^2}$ with a threshold δ on the intensity derivative in the gradient direction, $\Phi_1(x) = 0$ and $\Phi_2(x) = x\,\alpha_2$, where α_2 is a positive constant allowing a diffusion only in the minimal curvature direction.

2.2 Anisotropic Adaptive Filtering

In this section we describe a method developed for computer vision applications [7, 5]. This technique is an extension of the well-known Wiener filter and its adaptive extension (see [1]), and consists in an anisotropic filtering using local filter synthesis by means of an estimation of local orientation and the degree of anisotropy. In this sense, the filtering process related to unsharp masking [12] using the stationary Wiener filter solution as low pass and an adaptive high pass composed by a set of fixed filters.

Taken Abramatic and Silverman model [1] $H_\alpha = H + (1-\alpha)(1-H)$, with $H = \frac{S_{ff}}{S_{ff}+\sigma_n^2}$ is the Wiener filter with noise standard deviation σ_n and $0 \leq \alpha \leq 1$ the visibility function introduced by Abramatic and Silverman. Knutsson et al.[7] introduced an anisotropic component that allowed to control the level of anisotropy of 2D images with a factor γ

$$H_{\alpha,\gamma} = H + (1-\alpha)(\gamma + (1-\gamma)cos^2(\phi-\theta))(1-H) \tag{3}$$

where ϕ defines the angular direction of filter, θ is the orientation of local image structure, and directed anisotropy function $cos^2(\phi-\theta)$ is implemented as a steerable filter. Extending this solution to a multidimensional case with dimension N (see [14]), we have:

$$H_\gamma = H + (1-H) < \mathbf{C}, \mathbf{U} > \tag{4}$$

with, $\mathbf{C} = \sum_{k=1}^{N} \gamma_k \hat{\mathbf{e}}_k \hat{\mathbf{e}}_k{}^T$ the control tensor with eigenvalues γ_k and eigenvectors $\hat{\mathbf{e}}_k$, and $\mathbf{U} = \hat{\mathbf{u}}\hat{\mathbf{u}}^T$ outer product description of the Fourier domain with multidimensional frequency direction $\hat{\mathbf{u}}$ ($\hat{\mathbf{u}} = \frac{\mathbf{u}}{|\mathbf{u}|}$). Then, the control tensor is basically weighting, according to its shape, the components of the signal in the Fourier domain. The shape is given by its eigenvectors. High-pass frequency component is weighted by a projection of spatial frequencies over the principal axes of signal. In this sense we are reducing high frequency components in directions where spectrum is weak, because in those directions adaptive filter will mainly become

Wiener filter H, which is the low pass component. This kind of adaptive filter can be written as a linear combination of the Wiener filter and a set of fixed filters H_k in different directions $\hat{\mathbf{n}}_k$ (see [14, 3]), given by: $H_k(\mathbf{u}) = (1-H)(\mathbf{n}_k^T\hat{\mathbf{u}})^2$ getting another expression for equation (4):

$$H_c = H + \sum_{k=1}^{N(N+1)/2} < \mathbf{M}_k, \mathbf{C} > H_k$$

where the tensors $\mathbf{M}_k$ are defined by the outer product of filter directions $\hat{\mathbf{n}}_k\hat{\mathbf{n}}_k^T$. For a N-dimensional signal, the number of filters needed for this configuration is given by $N(N+1)/2$, because this is the number of independent components of control tensor $\mathbf{C}$, which is described by a symmetric $N \times N$ matrix. This yields 3 fixed directional for a 2D signal and 6 for 3D signal. Then, this scheme is based on the inner product of two tensors; $\mathbf{M}_k$, referred to the directions of filters and control tensor $\mathbf{C}$, obtained from the structure tensor $\mathbf{T}$ [7, 2]. To determine both tensors, we use the directions given by vectors pointing to the half of vertices of a polyhedron (a semi-hexagon for 2D, a semi-icosahedron, etc) [6] . These directions are enough to determine $\mathbf{M}_k$ and local structure tensor $\mathbf{T}$.

The structure tensor is obtained from combining quadrature filter responses, oriented in these directions [6]:

$$\mathbf{T} = \sum_{k=1}^{N(N+1)/2} \mathbf{M}_k |q_k|$$

with $|q_k|$ quadrature filter magnitude responses, using spherically separable quadrature filters $Q(\mathbf{u}) = R(\rho)D_k(\hat{\mathbf{u}})$, with $R(\rho) = e^{-(\frac{4}{B^2 ln2})(ln^2(\frac{\rho}{\rho_0}))}$ the radial function and $D_k = (\hat{\mathbf{u}}^T\hat{\mathbf{n}}_k)^2$ if $\hat{\mathbf{u}}^T\hat{\mathbf{n}}_k > 0$ and zero otherwise the directional function. We denote $\mathbf{u}$ the vector valued frequency variable, $\rho = \| \mathbf{u} \|$, $\hat{\mathbf{u}} = \frac{\mathbf{u}}{|\mathbf{u}|}$, ρ_0 the center frequency and B the relative bandwidth in octaves.

This tensor is symmetric and real and can be written as a weighted sum of outer products of its orthogonal eigenvectors, being its eigenvectors the principal axes of the local signal spectrum. The control tensor $\mathbf{C}$ can be obtained as a normalization of $\mathbf{T}$, that is, $\mathbf{C}$ has the same eigenvectors as $\mathbf{T}$ but with normalized eigenvalues. Then, $\mathbf{C}$ can be obtained as $\mathbf{C} = \frac{\lambda_1}{\lambda_1^2+\sigma_a^2}\mathbf{T}$, where λ_1 is the maximum eigenvalue of $\mathbf{T}$, and σ_a is a term defining the trade-off between resolution and stability. That is, for $\sigma_a = 0$ it provides maximum resolution, and the larger σ_a is, the smoother Wiener solution will be. However, the smaller λ_1, the smoother the final filter, thus getting maximum resolution when λ_1 is large compared with σ_a. In our implementation [4, 14], we have used a more general way to get control tensor $\mathbf{C}$ given by:

$$\mathbf{C} = m(\lambda_1^{'})\mathbf{T}'$$

where $m(\lambda_1^{'}) = \gamma(1-\lambda_1^{'}) + \frac{\lambda_1^{'\beta_a}}{\lambda_1^{'(\alpha+\beta_a)}+\sigma_a^{\beta_a}}$ is called mapping function and $\mathbf{T}'$ is the local structure tensor with eigenvalues $\lambda_1^{'}$ and normalized with the globally largest λ_1. The values of α, β_a, γ and σ_a control the shape of function $m(\lambda_1^{'})$

and therefore weight high frequencies. σ_a can be considered as a soft measure noise-signal transition area, α controls how peaky the curve is, β_a controls the transition speed of $m(\lambda_1^{'})$ and γ determines where the function starts for zero input.

3 Orientation extraction

In this section, we compare, on 3D synthetic images, the orientations obtained by the gradient of the smoothed image $\mathbf{e}_g$ and the maximal and minimal curvature directions $\mathbf{e}_M$ and $\mathbf{e}_m$ with the orientations obtained by the eigenvectors of the structure tensor, denoted $\mathbf{e}_{\lambda_1}, \mathbf{e}_{\lambda_2}, \mathbf{e}_{\lambda_3}$ and ordered decreasingly according to associated eigenvalues.

We use two synthetic 3D images to test these orientations. The first one is a synthetic 3D junction of vessels and the second one is a synthetic 3D hip joint (fig. 3). The intensity of the synthetic junction is 100 while the background

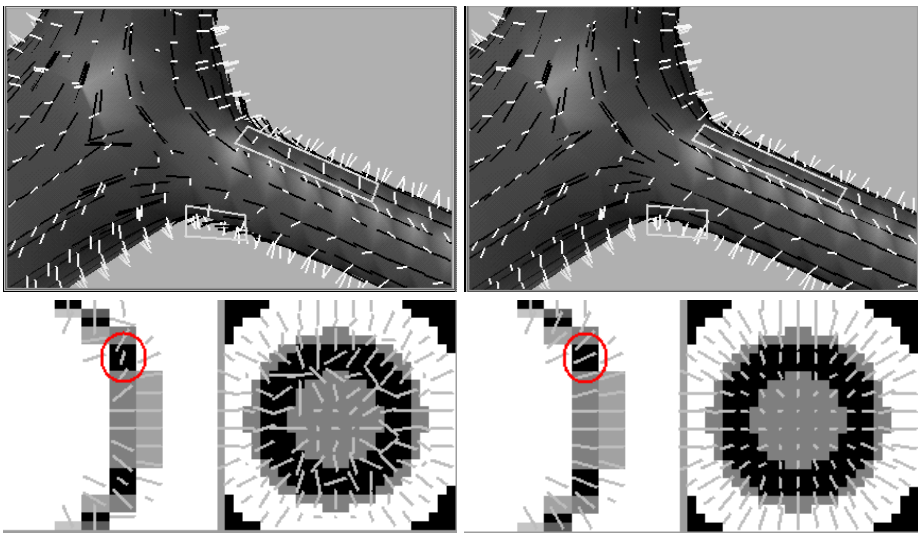

Fig. 1. Top row, Comparison of the estimated orientations on a synthetic 3D junction. Bottom row, Comparison of the estimated orientations on a synthetic 3D joint, where each image represents a YZ slice on the left and a XY slice on the right. Left column shows orientation obtained by the gradient and the minimal curvature, and right columns shows the first and the last eigenvectors of the structure tensor.

is 0, and the vessel radii are 4,3 and 2 voxels. The image has been convolved with a Gaussian kernel of standard deviation 1 and a white Gaussian noise of standard deviation 30 has been added (see top left of fig. 3). Top row of fig. 1 shows results of $\mathbf{e}_g$ in white and $\mathbf{e}_m$ in black on the left, computed with $\sigma = 2$, and $\mathbf{e}_{\lambda_1}$ in white and $\mathbf{e}_{\lambda_3}$ in black on the right, computed with $\rho_0 = 1.52$ and $B = 2$. For both direction estimations, the results on the two widest vessels are very similar. However, the orientations are different near the junction and on

the smallest vessel. On the one hand, the top white square on the two images shows points of the surface where $\mathbf{e}_g$ gives much better results than $\mathbf{e}_{\lambda_1}$. In this case, while the vectors $\mathbf{e}_g$ are well oriented, the vectors $\mathbf{e}_{\lambda_1}$ are parallel to the point of view of the projection and seem very small. This can be explained by a global deviation of $\mathbf{e}_{\lambda_1}$ in the direction orthogonal to the 3D plane that contains the junction, which is globally the direction of maximal intensity variation. On the other hand, the bottom small white square shows that the black vectors $\mathbf{e}_{\lambda_3}$ are better oriented than $\mathbf{e}_m$, due to the Gaussian smoothing that displaces the contour position. Globally, the basis of the gradient direction and the principal curvature directions gives a better orientation estimation that the basis of the structure tensor eigenvectors.

In the second case, we present a synthetic hip joint (see bottom row of fig. 3) with a sphere and a semi-cylinder that simulate femoral head and hip. This 3D image has a size of $40 \times 40 \times 23$ and a $1 \times 1 \times 3.04$ voxel size. It has been generated with a binary image using the same parameter values as the synthetic junction and a noise standard deviation of 10. We observe (fig. 1 bottom row) a better orientation of $\mathbf{e}_{\lambda_1}$, computed with $\rho_0 = 0.785$ and $B = 2$, (see XY slice and circle in the YZ slice) than $\mathbf{e}_g$, computed with $\sigma = 1$. This better definition of the local structure is due to the fact that the gradient is very weak between the sphere and the semi-cylinder, so the normalized gradient orientation is not accurate. However, the tensor structure responds well in this case and points at the right direction.

4 Restoration

An intuitive analogy can be done between the two filtering techniques. First, the low pass filter used by the first one is a heat diffusion equation with a data attachment while the second one uses a Wiener filter. Second, anisotropic diffusion uses a diffusion function based on threshold parameter δ on the first derivative of intensity in the gradient direction to decide whether a region should be enhanced or smoothed. The proposed adaptive filtering uses a mapping function based on the first eigenvalue of the structure tensor to decide whether high frequencies should be increased or decreased. In this section, we compare restoration of noisy synthetic and real images using both methods.

4.1 Synthetic Images

Three synthetic images were created. The first one corresponds to two close bar-like structures, the second one to a 3D junction between vessels, and the third one to a synthetic joint. The first synthetic image is a 3D image of size $15 \times 15 \times 60$ containing two bar-like structures of width 3 voxels separated by 2 voxels. This image varies only along z axis and we represented an intensity profile at the center of XY plane and along Z axis in figure 2. The image was first convolved with a Gaussian of standard deviation 1 and then a Gaussian white noise of standard deviation 15 was added. Figure 2 left shows the intensity profile of the binary image that we created in plain line, and the convolved image in slashed line. Figure 2 middle shows the restored image after anisotropic

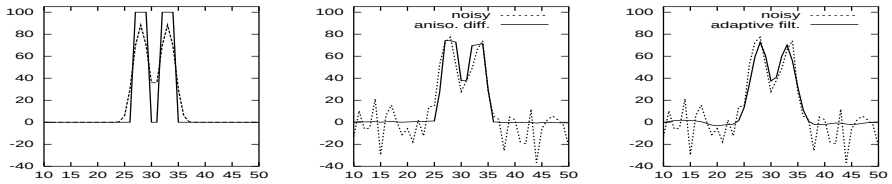

Fig. 2. Intensity profiles on a synthetic image.

diffusion ($\sigma = 1, \delta = 7, \beta = 0.05, \alpha_2 = 1$) superimposed on the noisy image. Figure 2 right shows the noisy image in slashed line and the restored image after adaptive filtering ($\alpha = \gamma = 0, \beta_a = 10, \sigma_a = 0.9$) in plain line. We remark that the adaptive filtering tends to give a result that is closer to the convolved image, and that the anisotropic diffusion attempts to converge to a segmented image with constant areas. Top row of fig. 3 represents a 3D synthetic junction

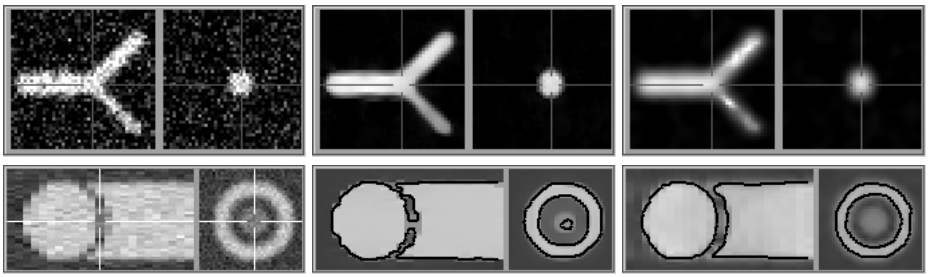

Fig. 3. Top row, comparison of the filtering on a synthetic 3D junction. Bottom row, comparison of the filtering on a 3D joint. Left, initial image with noise; middle, restoration using anisotropic diffusion; right, restoration using adaptive filtering.

between vessels. This image was described in section 3. We use the following definition of the Signal To Noise Ration (SNR): $SNR(I) = 10\ log_{10} \frac{\sigma^2(I)}{\sigma^2(I_b - I)}$ where I_r is the image to evaluate, I_b is the initial binary image, and σ denote the standard deviation. Its value is 0.4 for the noisy image, 5.7 for the image restored by anisotropic diffusion ($\sigma = 1, \delta = 10, \beta = 0.1, \alpha_2 = 1$) and 2.0 for the image restored by adaptive filtering ($\alpha = \gamma = 0, \beta_a = 10, \sigma_a = 0.9$). This means that we can obtain a better restoration using the anisotropic diffusion which corresponds to the visual impression in fig. 3 and which can be explained by the better estimation of the directions using the gradient and the principal curvature directions.

Bottom row of fig. 3 represents a 3D synthetic joint. This image was described in section 3. The parameters used for the anisotropic diffusion are $\sigma = 1, \delta = 10, \beta = 0.05, \alpha_2 = 1$ and for the adaptive filtering are $\alpha = \gamma = 0, \beta_a = 2, \sigma_a = 0.9$. A iso-intensity contour of threshold 60 was superimposed in black on the restored images to show that the adaptive filtering allows a better contrast enhancement. This is coherent with the better estimation of the orientations obtained by the structure tensor.

4.2 Real Images

Figure 4 presents results on two reals images. Top row is a XY slice representation of a $94 \times 52 \times 26$ sub-volume from a 3D Magnetic Resonance Angiography. The voxel size is $0.93 \times 0.93 \times 1.5mm$. We remark that the anisotropic diffusion ($\sigma = 1, \delta = 5, \beta = 0.2, \alpha_2 = 0.3$) provides a more homogeneous background than the adaptive filtering ($\alpha = \gamma = 0.5, \beta_a = 1.5, \sigma_a = 0.5$), while the conservation of the small vessels is similar. This conservation depends on the parameters of each method. Bottom row presents a $85 \times 83 \times 20$ sub-volume of a hip joint CT scan of voxel size $0.82 \times 0.82 \times 3mm$. We represent on the top left of each image a zoom on the joint region that confirms the better enhancement obtained by the adaptive filtering ($\alpha = \gamma = 0.5, \beta_a = 1.5, \sigma_a = 0.1$) compared to anisotropic diffusion ($\sigma = 1, \delta = 30, \beta = 0.1, \alpha_2 = 1$) as with the synthetic data.

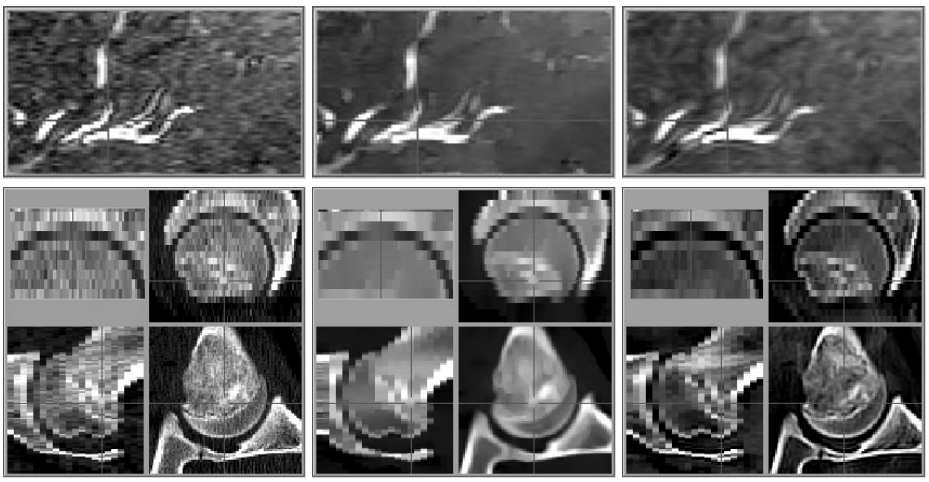

Fig. 4. Top row, 3D Magnetic Resonance Angiography. Bottom row, hip joint CT scan. Left, initial real image; middle, restoration using anisotropic diffusion; right, restoration using adaptive filtering.

5 Discussion and future work

We presented a comparison between two different types of anisotropic filtering. The first one uses the gradient and the principal curvature directions to lead the diffusion and the second one uses the eigenvectors of the structure tensor to weight the frequencies. We first compared the orientations used by each method and showed on synthetic 3D images that the gradient and principal curvature directions are better oriented in the case of vascular structures while the eigenvectors of the structure tensor respond better in regions of closed structures. We also made a qualitative comparison between the filtering results on both synthetic and real images applied to vessels and hip joint. As far as we know, this work is a first comparison that have been done between these two distinct filtering methods. In future works, we plan to make a quantitative evaluation of

the results. This evaluation should be done using the same best orientation estimation in both methods, according to the application. It also requires a specific segmentation algorithm and manually segmented images from physicians.

Acknowledgements

Thanks to Luis Alvarez for receiving the second author as a post-doctoral grant.

References

1. Abramatic,J.F. and Silverman M. Nonlinear restoration of noisy images. *IEEE Trans. of Pattern Analysis and Machine Intelligence*, 4(2):141–149, 1982.
2. J. Bigün, G. H. Granlund, and J. Wiklund. Multidimensional orientation: texture analysis and optical flow. *IEEE Transactions on Pattern Analysis and Machine Intelligence*, PAMI–13(8), August 1991.
3. Editor-in-Chief Isaac N.Bankman. *HandBook of Medical Imaging. Processing and Analysis.* Academic Press. ISBN 0-12-077790-8, 2000.
4. Granlund G.H. and Knutsson Hans. *Signal Processing for Computer Graphics.* Kluwer Academic Publishers. ISBN 0-7923-9530-1, 1995.
5. H. Knutsson, L. Haglund, H. Bårman, and G. H. Granlund. A framework for anisotropic adaptive filtering and analysis of image sequences and volumes. In *Proceedings ICASSP-92*, San Fransisco, CA, USA, March 1992. IEEE.
6. Knutsson, H. Representing local structure using tensors. In *6th Scandinavian Conference on Image Analysis. Oulu, Finland*, pages 244–251, 1989.
7. Knutsson,H., Wilson, R. and Granlund,G.H. Anisotropic non-stationary image estimation and its applications-part i: Restoration of noisy images. *IEEE Trans. on Communications. COM-31*, 3:388–397, 1983.
8. K. Krissian. Flux-based anisotropic diffusion: application to enhancement of 3d angiographies. Technical Report 0011, Instituto Universitario de Ciencias y Tecnologías Cibernéticas, Campus de Tafira, 35017 Las Palmas, España, Dec. 2000.
9. K. Krissian. *Traitement multi-échelle: applications à l'imagerie médicale et à la détection tridimensionnelle de vaisseaux.* PhD thesis, Univ. de Nice-Sophia Antipolis, Av. Joseph Vallot, 06108 Nice cedex 2, 2000.
10. K. Krissian, G. Malandain, and N. Ayache. Directional anisotropic diffusion applied to segmentation of vessels in 3d images. In *Scale-Space Theory in Computer Vision (Scale-Space)*, volume 1252 of *Lecture Notes in Computer Science*, pages 345–348, Utrecht, The Netherlands, July 1997. Springer Verlag.
11. P. Perona and J. Malik. Scale-Space and edge detection using anisotropic diffusion. *IEEE Trans. on Pattern Analysis and Machine Intel.*, 12(7):629–639, July 1990.
12. Schriber,W.F. Wirephoto quality improvement by unsharp masking. *J.Pattern Recognition*, 2:117–121, 1970.
13. J. Weickert. *Anisotropic Diffusion in image processing.* Teubner-Verlag, Stuttgart, 1998.
14. Westin et al. Affine adaptive filtering of CT data. *Medical Image Analysis*, 4:161–177, 2000.